JOURNAL OF MATERIALS SCIENCE 31 (1996) 2523–2529

Effect of thermal residual stress on the crack path in adhesively bonded joints

H. R. DAGHYANI, L. YE*, Y.-W. MAI
Centre for Advanced Materials Technology (CAMT), Department of Mechanical and Mechatronic Engineering, The University of Sydney, New South Wales 2006, Australia

Mode I fracture behaviour of adhesively bonded double and cantilever beam (DCB) compact tension (CT) joints was studied using a rubber-modified epoxy (Araldite® GY260) as the adhesive. Adherends were prepared from a carbon fibre (CF)/epoxy composite or aluminium alloys. The crack path in the joints was studied based on the sign of the non-singular *T*-stress ahead of the crack tip by calculating the thermal residual stress in the joints using finite element analysis. The results indicate that the type of adherend materials influence the level of the thermal residual stress in the adhesive layer, which consequently causes different crack paths in the joints, i.e. a uniformly smooth fracture surface in both CT and DCB aluminium joints and a wavy crack growth in the DCB CF/epoxy composite joints. However, the fracture energies of different types of adhesive joints were almost identical to each other for bond thickness $t < 0.2$ mm, and a somewhat higher fracture resistance was obtained for the CF/epoxy DCB joints with large bond thickness.

1. Introduction

It is well-known that cracks in adhesive joints propagate in a variety of ways depending on the remote loading conditions and the local stress state, the size and location of pre-existing flaws, the integrity of the interfacial bonding and the type of adhesive and the adherend. The actual crack path influences the strength of the joint and thus the nature of the crack path determines the effective fracture toughness of the adhesive bond [1–3]. It has been generally observed that a crack may grow within the adhesive, along the interface of the adhesive and the substrate, alternating between the adherend and the adhesive or alternating between two interfaces [1–9]. The fracture of isotropic materials occurs predominantly in a local opening mode, because this generally requires less fracture energy. However, the mismatch of material properties in the bonded joints may influence the local crack-tip stress field and induce different local stress intensity factors from its global remote loading. For example, a pure remote mode I loading applied on a layered material with an interfacial crack may induce a mixed-mode local stress field at the crack tip [2, 3]. This may cause the crack to deviate from its original direction. For adhesive joints, when the crack exists within the adhesive layer rather than at the adhesive/adherend interface, it is observed that [3, 6, 7, 9, 10] the crack may run within the adhesive layer or veer towards the interface or into the substrate depending on the remote loading mode and the local stress state. In addition, the crack path may also be influenced by the sign and the magnitude of the thermal residual stresses in the adhesive layer which have arisen from the difference in thermal expansion between the adhesive and the substrates.

In this study a rubber-modified epoxy was used to bond the aluminium substrates as well as the carbon-fibre/epoxy (CF/epoxy) composite adherends to study the effects of the adherend materials and the resulting thermal stress on the fracture behaviour of these joints with different bond thickness under remote mode I loading. The fracture behaviour of the modified epoxy used here has already been characterized for modes I and II fractures using aluminium as adherends as well as mixed-mode fractures using CF/Epoxy composite adherends in our previous papers [7, 10–12].

2. Experimental procedure

The base adhesive material was a diglycidyl ether of bisphenol A (DGEBA) epoxy resin (Araldite® GY260, Ciba-Geigy, Australia) modified with a liquid rubber system (CTBN, 1300 X 13, BF Goodrich, USA). The property profile of the adhesive material has been reported elsewhere [13]. It was found that the fracture energy of the pure GY260 epoxy resin was maximized by adding only 2% rubber and shear yielding was the major toughening mechanism of the bulk adhesive material. The composite adherends of double cantilever beam (DCB) specimens (Fig. 1a) were prepared using unidirectional carbon fibre/epoxy composite panels (320 mm × 300 mm × 2.3 mm), consisting of 16 layers of prepreg (5218 T300 BASF, USA), which were

*Author to whom all correspondence should be addressed.

0022–2461

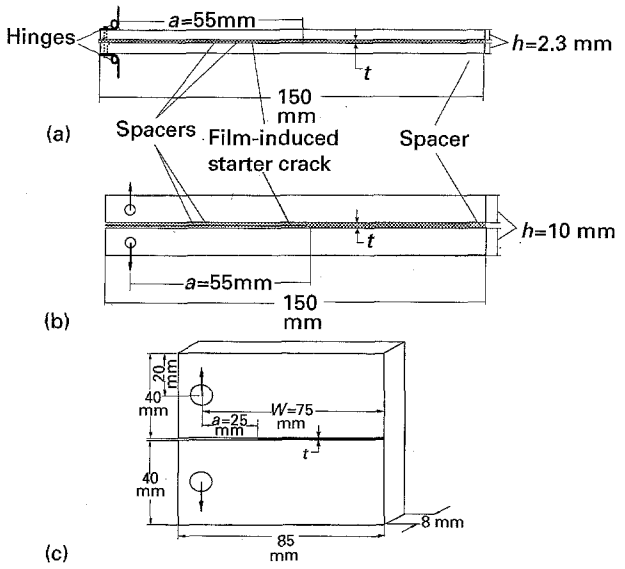

Figure 1 Schematic drawings of CT and DCB adhesive joints: (a) CF/epoxy, (b, c) aluminium specimens, t is the bond thickness.

processed using an autoclave according to the manufacturer's specification. After curing, the panels were cut to 20 mm × 150 mm strips as adherends. The bond surfaces were treated using a procedure described elsewhere [7]. The aluminium adherends for compact tension (CT) and DCB adhesive joints (Fig. 1b and c) were cut from 6061 aluminium alloy panels of 8 mm thickness and 6060-T5 aluminium alloy bars of 25 mm width and 10 mm height, respectively. The surfaces of the aluminium adherends to be bonded were treated using the P2 etching procedure as described elsewhere [14]. A 25 μm UPILEX® film, coated with the FREKOTE®-44 release agent was used to generate a film-induced starting crack in the middle of the adhesive layer for both DCB and CT specimens. The bond thickness (from 0.05–0.6 mm) of the adhesive joints was controlled by spacers located at both ends of the bond line as shown in Fig. 1. All sides of the bond line were sealed by a sticky tape except for a small opening. The epoxy resin was then cast through this opening and the joints were finally cured for 16 h at 120 °C. After curing, the edges of the bond line were polished. The edges of both CF/epoxy and aluminium-epoxy DCB specimens were coated with typewriter correction fluid and a travelling microscope was used to observe the crack growth along the bond line. Two hinges were attached to the end of the CF/epoxy DCB adherend beams for easy loading, and holes of 6 mm diameter were drilled near one end of the aluminium adherend DCB joints for pin-loading (Fig. 1b). The specimens were loaded in a 4302 Instron machine with a crosshead speed of 0.3 mm min^{-1}. The load–displacement curves were recorded continuously, and the crack lengths were marked every 5 mm on these records for the CF/epoxy composite joints. Unstable fracture occurred in both CT and DCB aluminium joints, and thus the maximum fracture load was used to evaluate the fracture toughness. After testing, the crack path in the specimens was examined using optical microscopy (OM).

3. Crack growth in adhesive joints

The major paths of crack growth in adhesively bonded joints have been investigated previously by many researchers [1, 3, 4, 6]. Their characteristics can be summarized as follows.

(a) An interfacial crack exists at the interface of the adhesive and the substrate (Fig. 2a.) The crack path is dependent on a number of variables including the toughness of interfacial bonding, the location and size of the pre-existing defects at the tip of the interfacial crack, the global and local stress intensity factors. The crack growth behaviour has been explained in previous quantitative studies [3, 15] which have introduced some useful parameters. When an adhesive joint contains an interfacial crack, which is under remote loading K_I^∞ and K_{II}^∞, the remote loading phase angle, ϕ, is defined as

$$\phi = \arctan\left(\frac{K_{II}^\infty}{K_I^\infty}\right) \tag{1}$$

The elastic mismatch between two dissimilar materials is governed by the following parameters under plane strain conditions [15]

$$\alpha = \frac{(1-\nu_2)/\mu_2 - (1-\nu_1)/\mu_1}{(1-\nu_2)/\mu_2 + (1-\nu_1)/\mu_1}$$

$$\beta = \tfrac{1}{2}\frac{(1-2\nu_2)/\mu_2 - (1-2\nu_1)/\mu_1}{(1-\nu_2)/\mu_2 + (1-\nu_1)/\mu_1} \tag{2}$$

$$\varepsilon = \frac{1}{2\pi}\ln\left(\frac{1-\beta}{1+\beta}\right)$$

where μ is the shear modulus, ν is Poisson's ratio, subscripts 1 and 2 refer to the substrate and the adhesive, respectively, and ε is the oscillatory index. The mismatch between the two materials at the tip of an interfacial crack causes local stress intensity factors, K_I^k and K_{II}^k, and a local phase angle, ψ, defined by

$$\psi = \arctan\left[\frac{\mathrm{Im}(Kl^{*i\varepsilon})}{\mathrm{Re}(Kl^{*i\varepsilon})}\right] \tag{3}$$

where K is the complex interfacial stress intensity factor and l^* is the distance from the crack tip where the local stress intensity factors are defined. A putative kink-like flaw caused by either defects such as dusts and bubbles or surface roughness of the substrate during bonding may exist at the tip of the interfacial crack. The necessary condition for the interfacial crack to kink, i.e. to deviate from the interface, is that the local stress intensity factors at the tip of the kink, K_I^k and K_{II}^k, satisfy the conditions $K_{II}^k \geq 0$ and $K_I^k > 0$. When $K_{II}^k < 0$, the kinked crack is reflected back to the interface [4]. The sufficient condition for the interfacial crack to veer out of the interface of toughness $\Gamma_I(\psi)$ into an adjacent material of toughness Γ_s is given by [16]

$$\frac{\Gamma_I(\psi)}{\Gamma_S} \geq \frac{G_I}{G_S} \tag{4}$$

where G_I is the strain energy release rate along the interface and G_S is the strain energy release rate at the tip of a kink which satisfies the condition of $K_{II}^k = 0$.

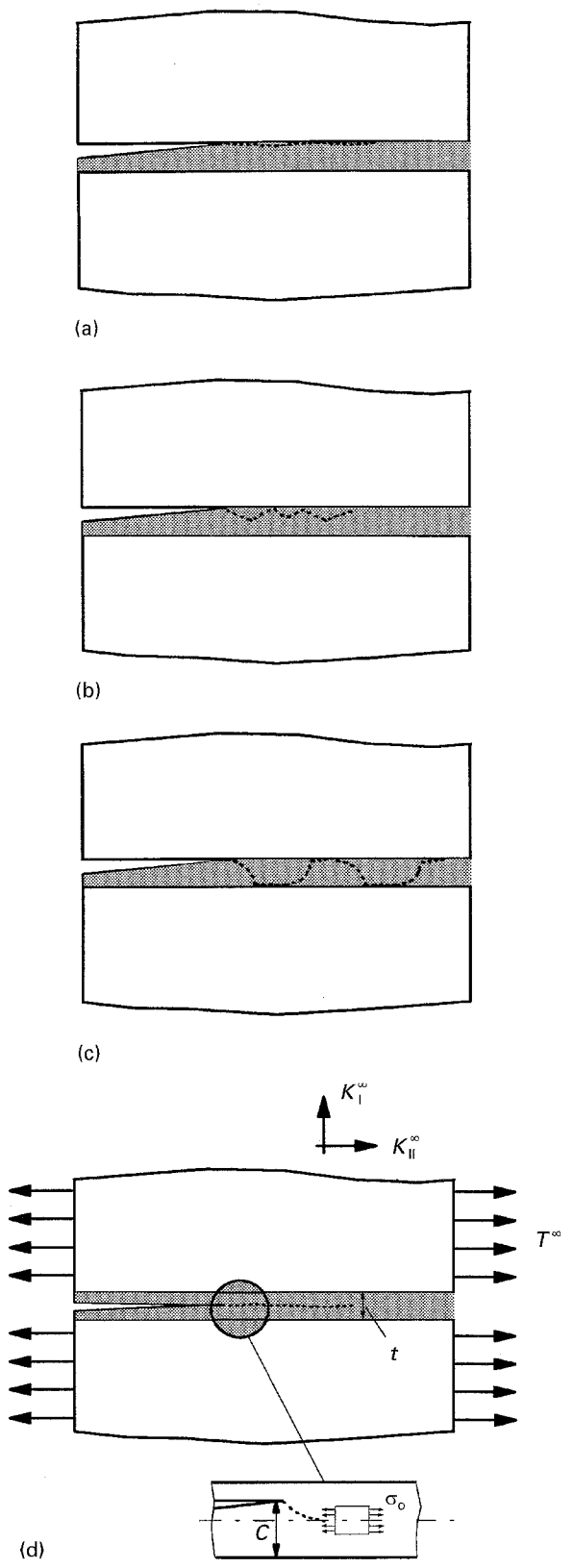

Figure 2 Major crack paths for adhesive joints: (a) interfacial crack, (b) serrated crack, (c) alternating crack, and (d) in-layer crack.

When the crack propagates along the interface without kinking into the adhesive layer, the interfacial toughness essentially increases as the proportion of global shear loading increases [1]. No effect of the thermal residual stress on the interfacial fracture toughness has been identified in all previous observations [1, 6–9, 17]. For poor interfacial bonding, however, the crack will remain at the interface regardless of the variation in the remote phase angle, ϕ [6].

(b) A serrated crack path (Fig. 2b) may occur when the conditions for crack veering into the adhesive layer and kinking back towards the interface are provided. That is when $K_{II}^k \geq 0$, the interfacial crack veers into the adhesive layer. But when the condition of $K_{II}^k < 0$ is gradually satisfied at the tip of the kinked crack, it is reflected back to the interface [4] and a serrated crack path is produced. The fracture toughness of such crack propagation was observed to be approximately 20% greater than that of the interfacial crack propagation [1]. For such a crack path, by increasing the magnitude of thermal residual stress, the fracture toughness was slightly increased [1].

(c) Fig. 2c shows an alternating crack path observed in the aluminium–epoxy adhesive joints [1, 5] whereby the crack deviated from one interface across the adhesive layer towards the opposite interface. Akisanya and Fleck [4] have analysed the alternating crack path by finite element method and showed that the local phase angle, ψ, of the interfacial pre-crack increases with crack growth under a fixed remote loading, K^∞, and a thermal residual stress, σ_0, of the interfacial crack. This causes the interfacial crack to veer into the adhesive layer when the interfacial local phase angle, ψ, at the crack tip attains a critical value, ψ_c [16]. The fracture toughness measured in a specimen with an alternating crack path under remote mode I loading was observed to increase approximately two-fold compared to an interfacial crack [1].

(d) A pre-crack exists in the centre of the bond line or slightly above the centre line (Fig. 2d). Cotterell and Rice [18] postulated that the crack trajectory is dependent on the sign of the local non-singular stress, T, acting parallel to the crack plane. The local T-stress is dependent on all four remote loading parameters which is given by [3]

$$T = \frac{1-\alpha}{1+\alpha} T^\infty + \sigma_0 + c_I \frac{K_I^\infty}{t^{1/2}} + c_{II} \frac{K_{II}^\infty}{t^{1/2}} \quad (5)$$

where T^∞ is the remote non-singular stress acting parallel to the crack plane, σ_0, the thermal residual stress, c_I and c_{II}, coefficients depending on the location of the in-layer pre-existing crack given by Fleck *et al.* [3], and t the adhesive thickness. The local and global stress intensity factors are related to the strain energy release rate, G, by [3]

$$G_I = \frac{1}{E_a}(K_I^{k2} + K_{II}^{k2}) = \frac{1}{E_S}(K_I^{\infty 2} + K_{II}^{\infty 2}) \quad (6)$$

where E_a and E_s are Young's modulus of the adhesive and the substrate, respectively. Equation (6) is equivalent to

$$K_I^k = \left(\frac{1-\alpha}{1-\beta}\right)^{1/2} (K_I^\infty \cos\Phi - K_{II}^\infty \sin\Phi)$$
$$K_{II}^k = \left(\frac{1-\alpha}{1-\beta}\right)^{1/2} (K_I^\infty \sin\Phi + K_{II}^\infty \cos\Phi) \quad (7)$$

where the phase angle Φ is a dimensionless function of the elastic mismatch constants (α and β) and the location of an in-layer crack, c parallel to the interface,

i.e. $\Phi = \Phi\ (c/t, \alpha, \beta)$ which is a phase angle shift between the remote and the local stress intensities [3]

$$\Phi = \arctan\left(\frac{K_{II}^{k}}{K_{I}^{k}}\right) - \arctan\left(\frac{K_{II}^{\infty}}{K_{I}^{\infty}}\right) \quad (8)$$

For different material combinations, Φ is given by Fleck *et al.* [3].

Another controlling parameter which affects the nature of the crack trajectory is related to the variation of the mode II stress intensity factor across the bond thickness. For a predominant mode I remote loading ($K_{II}^{\infty} = 0$), the centre line of the adhesive is a path satisfying the condition of $K_{II}^{k} = 0$. However, if the crack lies above the interface, the crack will veer towards the centre line if $K_{II}^{k} > 0$ [3]. Four different possible patterns of crack propagation can occur depending on the sign of T and $\partial K_{II}^{k}/\partial c$ [3]. When $\partial K_{II}^{k}/\partial c > 0$ and $T < 0$, an off-centre pre-crack will veer towards the centre line and run stably along that line because of the positive K_{II}^{k}. Then the compressive T-stress will stabilize the crack path in the centre line, as illustrated in Fig. 3a. The crack trajectory is expected to be wavy along the centre line if $\partial K_{II}^{k}/\partial c > 0$ and $T > 0$. The positive K_{II}^{k} drives the crack towards the centre line, but the tensile T-stress destabilizes the crack trajectory in the centre line. A positive $\partial K_{II}^{k}/\partial c$ may keep the crack in the centre line if T is relatively small. Consequently, a wavy crack pattern is expected to occur along the centre line. However, the crack will deviate towards the interface if T is large enough (Fig. 3b). The crack is expected to kink gradually towards the interface when both $\partial K_{II}^{k}/\partial c$ and T are negative (Fig. 3c), while for negative $\partial K_{II}^{k}/\partial c$ and positive T, the crack will run in an unstable manner with a large angle towards the interface (Fig. 3d). The sign of $\partial K_{II}^{k}/\partial c$ can be obtained from Equation 7 which is dependent only on the elastic mismatch parameters α and β. Fracture propagation in the adhesive occurs when the local stress intensity factor, K_{I}^{k}, at the crack tip achieves the fracture toughness of the adhesive joint, K_{IC}. The T-stress is thus calculated from Equation 5 considering $K_{II}^{\infty} = 0$, and using Equation 6, gives

$$T = \frac{1-\alpha}{1+\alpha} T^{\infty} + \sigma_0 + \left(\frac{E_s}{E_a}\right)^{1/2} c_I \frac{K_{IC}}{t^{1/2}} \quad (9)$$

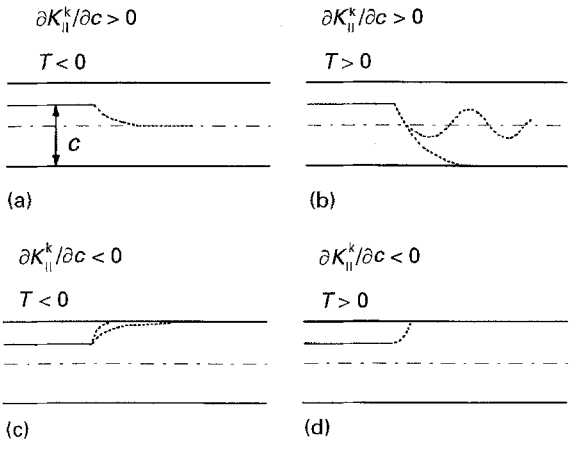

Figure 3 Different patterns of crack paths for in-layer crack propagation: (a) $\partial K_{II}^{k}/\partial c > 0$ and $T < 0$, crack path along the centre line, (b) $\partial K_{II}^{k}/\partial c > 0$ and $T > 0$, a wavy crack path propagates along the centre line if T is relatively small, but the crack deviates towards the interface if T is enough large, (c) $\partial K_{II}^{k}/\partial c < 0$ and $T < 0$, crack kinks gradually towards the interface, and (d) $\partial K_{II}^{k}/\partial c < 0$ and $T > 0$, crack runs unstably with large angle towards the interface [3].

4. Evaluation of fracture energy

The strain energy release rate, G, of the CF/epoxy composite adhesive joints was evaluated based on the compliance equation obtained from the load–deflection curves of the DCB test specimens

$$G = \frac{P^2}{2b}\frac{dC}{da} \quad (10)$$

where P is the applied load, b the beam width, C the specimen compliance and a the crack length. Owing to the unstable fracture of aluminium–epoxy DCB joints, the maximum load at fracture, P_C, was used to evaluate G_{IC} which is given by [19]

$$G_{IC} = \frac{4P_C^2(3a^2 + h^2)}{E_s b^2 h^3} \quad (11)$$

where h is the thickness of the adherend. The fracture toughness of the CT joints, is given by [20]

$$K_{IC} = \frac{P_C}{bW^{1/2}}\left(\frac{E_a}{E_s}\right)^{1/2}[29.6(a/W)^{1/2} - 185.5(a/W)^{3/2} + 655.7(a/W)^{5/2} - 1017(a/W)^{7/2} + 638.9(a/W)^{9/2}] \quad (12)$$

where W is the width of the CT specimen (Fig. 1).

5. Results and discussion

A typical load–deflection curve of the DCB joints is shown in Fig. 4. Discrete load drops occurred in some cases associated with intermittent (stick–slip) crack jumps for the CF/epoxy specimens. The critical strain energy release rate, G_{IC}, was evaluated using Equation 10 based on a master compliance calibration curve obtained by fitting a polynomial to the C–a data of specimens with different bond thickness considering

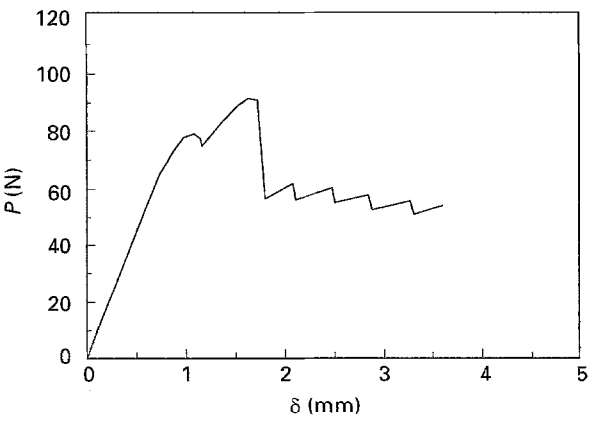

Figure 4 Typical load–deflection (p–δ) curve of DCB composite joints (t = 200 μm).

the small difference in the effect of the adhesive layer on the compliance is negligible (the largest deviation in flexural stiffness for the maximum bond thickness, $t = 0.5$ mm obtained from the modified beam theory is less than 0.5%). Fig. 5 shows the master compliance calibration curve and typical C–a data for some CF/epoxy specimens. As shown in Fig. 6, G_{IC} was almost a constant for each bond thickness as the crack grew. Thus, the fracture toughness of CF/epoxy DCB joints cited hereafter is the average value of G_{IC} obtained for different crack length. Because fracture was unstable for both CT and DCB aluminium joints, the maximum load was used to calculate G_{IC}. For CT joints, K_{IC} was first obtained from Equation 12, then G_{IC} was calculated from Equation 6 assuming $K_I^k = K_{IC}$ and $K_{II}^k = 0$, which is valid when the crack is located in the centre line of the adhesive ($c/t = 0.5$). When $c/t > 0.5$, $K_{II}^k \neq 0$, however, for predominantly remote mode I loading, K_{II}^k is very small compared to K_I^k (e.g. for $c/t = 0.75$, $K_{II}^k/K_I^k = 0.04$), thus, the assumption of $K_I^k = K_{IC}$ can be used with appropriate approximation. For aluminium DCB specimens, G_{IC} was directly evaluated from Equation 11. Fig. 7 shows the variation of G_{IC} as a function of bond thickness, t, for these three specimen geometries. G_{IC} was almost a constant for small bond thickness ($t < 0.2$ mm), but increased gradually for larger bond thickness. For CF/epoxy composite DCB specimens,

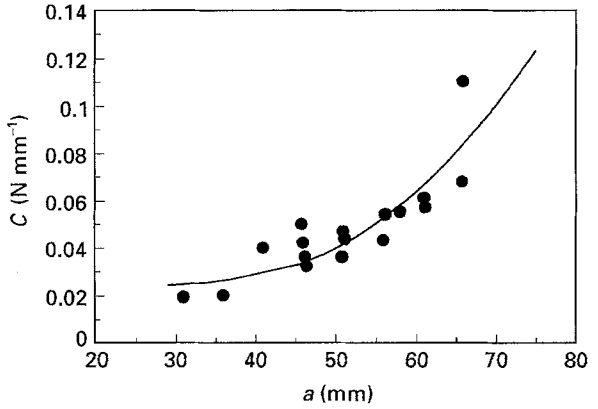

Figure 5 Master curve of compliance calibration in C–a plots.

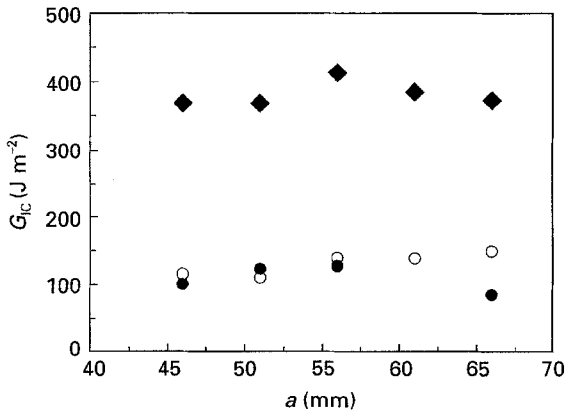

Figure 6 Critical strain energy release rate, G_{IC}, as a function of crack length in DCB CF/epoxy joints: (◆) $t = 0.5$ mm, (○) $t = 0.2$ mm, and (●) $t = 0.05$ mm.

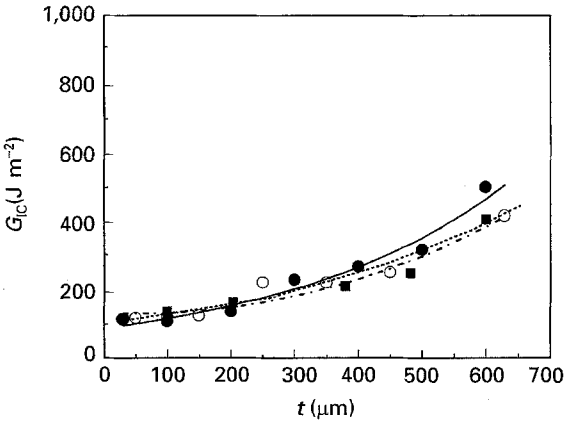

Figure 7 Variation of critical strain energy release rate, G_{IC}, versus bond thickness, t in DCB and CT geometries. (●) CF/epoxy DCB, (■) CT, (--○--) Al/CB.

G_{IC} was somewhat higher than that of the CT and DCB aluminium joints when $t > 0.2$ mm. Different fracture surface morphologies were also observed for these three specimen geometries. For stick–slip behaviour of the CF/epoxy DCB composite joints, the crack propagated first unstably causing a wavy path and then changed to a stable crack growth causing a rough region associated with some shear deformation. A mirror-like and featureless fracture surface was, however, observed for the CT and DCB specimens. Fig. 8 shows the crack path in the CT and DCB specimens where the crack was initiated from the film-induced pre-crack and propagated within the adhesive layer. Because of the difficulty in specimen preparation, the film-induced pre-crack was not precisely located in the centre line of the adhesive layer. For the CT and DCB aluminium adhesive joints used in this study, it has been found that $\alpha > 0$ and $\beta = \alpha/4$, being independent of specimen geometry, and thus, $\partial K_{II}^k/\partial c$ is positive [3]. Therefore, the crack growth was initiated from slightly upper (or lower) side of the centre line and then propagated towards the centre line as discussed in the previous sections with two different patterns: i.e. uniformly smooth for the CT and DCB aluminium joints (Fig. 3a) and wavy for the DCB CF/epoxy composite joints (Fig. 3b) along the centre line of the adhesive layer.

As discussed previously, the in-layer crack propagation in adhesive joints is attributed to the sign of the non-singular stress acting parallel to the crack surface at the crack tip, i.e. the T-stress [3]. The sign of the T-stress in the joints has been determined using Equation 9 in this work. The first term in Equation 9 is negligible compared with the other terms [3]. The thermal residual stress, σ_0 (second term), in the joints was evaluated using finite element models for the CT and DCB specimens. The value of the third term was calculated from the fracture toughness of the joints and the value of c_1 is obtained from the work of Fleck *et al.*

Two-dimensional finite element models (FEM) were generated to evaluate the thermal residual stress state along the bond line. All finite element analyses (FEA) were conducted with eight-noded quadrilateral plane

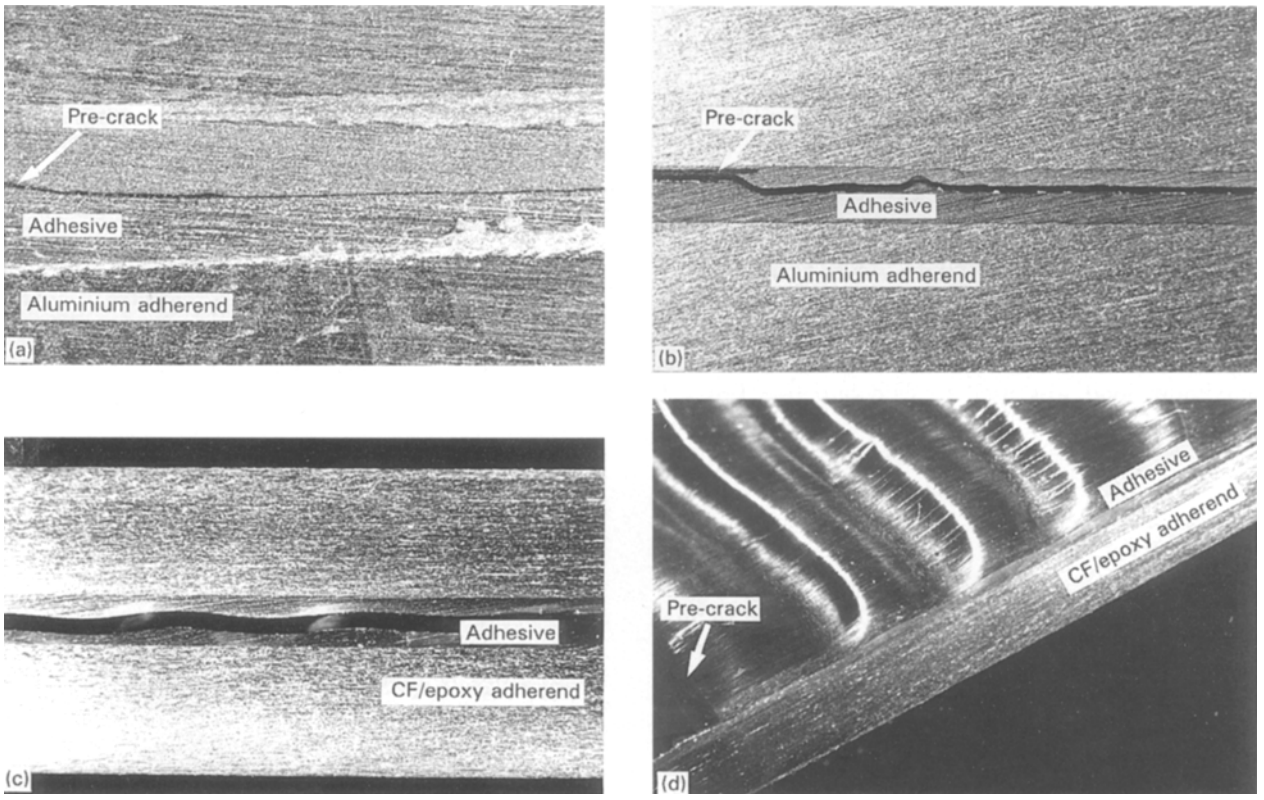

Figure 8 Crack paths in (a) CT aluminium-epoxy joint, (b) DCB aluminium-epoxy joints, and (c) a DCB composite adhesive joint; (d) fracture surface of a DCB composite. Crack growth is from left to right.

stress elements, assuming the adhesive to be plastic, the aluminium adherend elastic-perfect-plastic, and the composite adherend elastic. Some typical properties of the adhesive and the adherends are listed in Table I. All finite element analyses were carried out using the ADINA [21] software. It was assumed that at the curing temperature before cooling, the specimen was free of stress and the thermal residual stress was produced upon cooling because of the mismatch in thermal expansion between the adhesive and the adherend. Therefore, the FEM was subjected to a thermal loading with $\Delta T = -100\,^{\circ}C$, i.e. the difference between the ambient and the curing temperature of the adhesive joints.

The thermal residual stress (σ_0, see Fig. 2d) in each joint (CT or DCB) was almost constant along the bond line (except at the specimen edge) and independent of the bond thickness. However, due to the different coefficients of thermal expansions between the CF/epoxy (DCB) and aluminium (CT and DCB) adherends, different thermal stresses were obtained for these joints. The T-stress was evaluated for the three different joints and the results are shown in Table II. As discussed in Section 3, a negative T-stress leads the crack to propagate along the centre line of the adhesive layer. Thus, a uniformly smooth in-layer fracture surface was observed for the CT and DCB aluminium joints. The positive T-stress value for the DCB CF/epoxy composite joints resulted in a wavy crack (see Fig. 8) along the centre line of the adhesive layer. These observations were consistent with the prediction described in the previous section. Therefore, the type of the adherend material influences the level of the thermal residual stress in the adhesive layer and consequently causes different crack paths in the joints.

The wavy crack path in the DCB CF/epoxy composite joints was a dominant fracture morphology for

TABLE I Mechanical properties of adhesive and adherend

Material	Young's modulus E_{11} (GPa)	Transverse Young's modulus E_{22} (GPa)	Shear modulus μ (GPa)	Ultimate tensile strength, σ_u (MPa)
GY260 + 2% Rubber	3.15	–	1.6	81
Aluminium Alloy-6061	71	71	25.5	152 [22]
Aluminium Alloy-6060-T5	71	71	25.5	150 [22]
CF/epoxy 5218 T300	133	8.7	–	2194

TABLE II Results of T-stress obtained from thermal residual stress, σ_0, and adhesive fracture toughness, K_{IC}, for CT, DCB aluminium and DCB CF/epoxy composite adhesive joints

Specimen	σ_0 (MPa)	K_{IC} (MPa m$^{1/2}$) for t (mm)			T (MPa) for t (mm)		
		0.1	0.2	0.5	0.1	0.2	0.5
CT-Al	11	0.6	0.72	0.9	−15.8	−12	−7.2
DCB-Al	11	0.62	0.7	0.92	−16.1	−11.2	−7.6
DCB (CF/epoxy)	26.9	0.58	0.65	1.0	1.2	3	3.5

the specimens with bond thickness $t > 0.1$ mm. By increasing the bond thickness, the amplitude of the waves was increased, but the period of the waves was almost constant. The greater amplitude of the waves for larger bond thickness can be attributed to the relief of the constraint effect of the composite adherend and the relatively tough adhesive material ($G_C = 2.76\,kJ\,m^{-2}$ for bulk adhesive material). The wavy crack path also indicates that the crack propagates under a local mixed-mode loading. Thus, the mixed-mode stress state at the crack tip requires more energy for crack propagation compared to the local pure mode I loading. The increase of fracture energy of the DCB CF/epoxy composite joints in large bond thickness compared to that of the aluminium joints is caused by this energy dissipation mechanism.

6. Conclusions

The fracture behaviour and the crack paths in CT and DCB aluminium adhesive joints as well as DCB CF/epoxy composite adhesive joints with different bond thickness have been investigated. The fracture energy of the different types of joints was almost the same for the bond thickness $t < 0.2$ mm but the DCB composite joints showed somewhat higher fracture resistance for larger bond thickness. The pre-crack for both joint geometries was introduced near the centre line of the adhesive layer; however, a uniformly smooth fracture surface was observed for both CT and DCB aluminium joints, but a wavy crack propagation pattern appeared for the DCB CF/epoxy composite joints. The reason for the different crack paths was explained in terms of the sign for the non-singular T-stress ahead of the crack tip. The T-stress was determined from the thermal residual stress generated during the curing cycle using finite element models. It was found that for the aluminium adherends with different geometries, almost identical T-stresses are obtained, thus a similar crack path is expected. The results of the crack paths are consistent with theoretical predictions given elsewhere [3].

Acknowledgements

H. R. Daghyani was supported by a scholarship from the Ministry of Culture and Higher Education of Iran (MCHE). Partial support of this work by the Australian Research Council is appreciated.

References

1. A. R. AKISANYA and N. A. FLECK, *Int. J. Fract.* **58** (1992) 93.
2. M. CHARALAMBIDES, A. J. KINLOCH, Y. WANG and J. G. WILLIAMS, *ibid.* **54** (1992) 269.
3. N. A. FLECK, J. W. HUTCHINSON and Z. SUO, *Int. J. Solids Struct.* **27** (1991) 1683.
4. A. R. AKISANYA and N. A. FLECK, *Int. J. Fract.* **55** (1992) 29.
5. H. CHAI, *ibid.* **32** (1987) 211.
6. J. S. WANG and Z. SUO, *Acta Metall.* **38** (1990) 1279.
7. H. R. DAGHYANI, L. YE and Y.-W. MAI, *J. Compos. Mater.* (1996) in press.
8. H. C. CAO and A. G. EVANS, *Mech. Mater.* **7** (1989) 295.
9. M. D. THOULESS, *Acta Metall.* **38** (1990) 1135.
10. H. DAGHYANI, L. YE and Y.-W. MAI, *J. Adhesion* **53** (1995) 149.
11. *Idem, ibid.*, **53** (1995) 163.
12. *Idem, ibid.*, (1996) in press.
13. H. R. DAGHYANI, L. YE, Y.-W. MAI and J. WU, *J. Mater. Sci. Lett.* **13** (1994) 1330.
14. R. F. WEGMAN, in "Surface Preparation Techniques for Adhesive Bonding" (*Noyes*, 1989) pp. 9–27.
15. J. DUNDURS, *J. Appl. Mech.* **36** (1969) 650.
16. M.-Y. HE and J. W. HUTCHINSON, *J. Appl. Mech.* **56** (1989) 270.
17. K. M. LIECHTI and Y. S. CHAI, *ibid.* **59** (1992) 295.
18. B. COTTERELL and J. R. RICE, *Int. J. Fract.* **16** (1980) 155.
19. "Fracture Strength in Clevage of Adhesives in Bonded Joints", ASTM-D3433-75, Annual Book of ASTM Standards (American Society for Testing and Materials, Easton, MD, 1980).
20. Y.-W. MAI and A. S. VIPOND, *J. Mater. Sci. Lett.* **13** (1978) 2280.
21. ADINA R and D, Inc., USA (1992).
22. P. M. UNTERWEISER and H. M. COBB (eds), "Worldwide Guide to Equivalent Nonferrous Metals and Alloys", 2nd Edn, (ASM International, 1987).

Received 15 September
and accepted 25 October 1995